Transportation Research Part B 71 (2015) 194–212

Contents lists available at ScienceDirect

Transportation Research Part B

journal homepage: www.elsevier.com/locate/trb

Bidirectional pedestrian fundamental diagram

Gunnar Flötteröd [a,*], Gregor Lämmel [b]

[a] Department of Transport Science, KTH Royal Institute of Technology, Stockholm, Sweden
[b] Institute for Advanced Simulation, Forschungszentrum Jülich, Jülich, Germany

ARTICLE INFO

Article history:
Received 2 February 2014
Received in revised form 31 October 2014
Accepted 1 November 2014
Available online 27 November 2014

Keywords:
Bidirectional pedestrian flow
Fundamental diagram from first principles
Cellular automaton
Empirical validation

ABSTRACT

This article presents a new model of stationary bidirectional pedestrian flow. Starting out from microscopic first principles, a bidirectional fundamental diagram (FD) is derived that defines direction-specific flow rates as functions of direction-specific densities. The FD yields non-negative and bounded flows and guarantees that the instantaneous density changes that would result from these flows stay bounded between zero and jam density. In its minimal configuration, it uses just as many parameters as a unidirectional triangular FD: maximum walking speed, jam density, a collision avoidance parameter (from which the backward wave speed can be derived). A one-on-one mapping between the parameters guiding uni- and bidirectional pedestrian flows is proposed and both conceptually and empirically justified. Generalizations of the FD that maintain its desirable properties turn out to be straightforward by making its parameters density-dependent. The FD performs very well in comparisons against simulated and real data.

1. Introduction

The modeling of pedestrian traffic flow is relevant for the design and operation of pedestrian facilities as well as for emergency and evacuation planning. The present work exclusively focuses on the modeling of bidirectional flow. This phenomenon is separated from higher-level walking processes such as path following or route/destination choice by considering flows in long channels only. Within this scope, the following body of literature is of relevance.

1.1. Pedestrian cellular automata

The cellular automaton (CA) approach to pedestrian flow modeling has received much attention in the literature; Zheng et al. (2009) review more than 20 pedestrian CA models in the evacuation context. Pedestrian CAs were preceded by CAs for vehicular flow, initiated by the work of Nagel and Schreckenberg (1992), who introduce a CA model for single lane vehicular movements. The model yields realistic dynamics and a plausible fundamental diagram (FD). Exact and approximate expressions for different guises of this FD have been derived (Schadschneider, 1998). Rickert et al. (1996) extend the CA of Nagel and Schreckenberg (1992) into a two-lane model that allows for passing. Simon and Gutowitz (1998) introduce bidirectional flows into this model. Moussa (2008) also presents a CA model for bidirectional vehicular traffic. Daganzo (2006) establishes the equivalence of certain unidirectional CAs and the Kinematic Wave Model (KWM; Lighthill and Witham, 1955; Richards, 1956). Laval and Leclercq (2013) summarize this and other results under the umbrella of Hamilton–Jacobi theory.

* Corresponding author.
E-mail addresses: gunnar.floetteroed@abe.kth.se (G. Flötteröd), g.laemmel@fz-juelich.de (G. Lämmel).

http://dx.doi.org/10.1016/j.trb.2014.11.001
0191-2615/

Applications of CAs to the modeling of pedestrian flows began in the late 1990s. Blue and Adler (1998) present a unidirectional CA model for a multi-lane ring road. The pedestrians differ by their desired speed and can perform lane changes. This model produces an FD similar to that proposed by Weidmann (1993). Fukui and Ishibashi (1999) develop a bidirectional CA model. Conflicts (two pedestrians facing each other) are resolved by lateral movements. For low densities, the model exhibits lane formation behavior; as densities increase, it produces a rapid state transition from free flow to total jam. The bidirectional pedestrian CA proposed by Baek et al. (2009) exhibits the same phenomenon. Muramatsu et al. (1999) and Muramatsu and Nagatani (2000) investigate this state transition in detail, identifying a stable critical density for large systems. Blue and Adler (2000a) also specify a CA model for bidirectional pedestrian flow with multiple lanes. Apart from allowing for lateral movements, they also enable pedestrians to switch positions under dense conditions, avoiding the previously observed breakdowns. Blue and Adler (2000b) develop a four-directional extension of this model. Blue and Adler (2001) compare bidirectional FDs obtained from CA simulations to standard shapes found in the literature and identify the rate at which conflicting pedestrians move around each other as decisive for the shape of the FD. Tajima et al. (2002) present a CA for bidirectional flows in a channel with open boundary conditions. The model yields a triangular FD mapping entrance densities on total flows. Kirchner et al. (2003b); Kirchner et al. (2003a) introduce "friction" into a model of bidirectional flow, such that speed is reduced when conflicts occur. However, the model is evaluated for evacuation scenarios only, in which bidirectional flows rarely occur. Nowak and Schadschneider (2012) consider bidirectional pedestrian flows in channels with periodic and open boundary conditions and analyze quantitatively the occurrence of free flow, disordered flow, lane formation, and gridlock.

1.2. Cell-transmission models

The cell-transmission model (CTM) was introduced by Daganzo (1994, 1995) and Lebacque (1996) as a numerical solution scheme for the KWM. Asano et al. (2007) propose a multi-directional CTM of pedestrian flow that acknowledges speed reductions due to directional conflicts. Their approach is based on the use of a "conversion function" that turns a cell's multi-directional density into a unidirectional one, to which then the standard CTM's flow transmission rules are applied. However, no concrete functional form for this conversion function is given, and the presented simulation studies ignore multi-directional effects within the cells. Guo et al. (2011) specify a two-dimensional CTM of pedestrian evacuations. Directional conflicts are not explicitly modeled, but a congestion-dependent branch is included in the FD. Both studies present simulation results but do not validate those against real data. Hänseler et al. (2014) adopt the approach of Asano et al. (2007) in a model system for pedestrian flows in public walking areas. They observe a good performance of their model when calibrating it against real densities and travel times but acknowledge that the use of unidirectional flow propagation rules is a simplification.

1.3. Force-based models

Force-based models describe the movements of individual pedestrians in continuous space and time as the consequence of a force vector pointing to a destination location and repellent forces avoiding collisions. A prominent instance is the social force model (Helbing and Molnár, 1995; Helbing et al., 2000), where the repellent forces depend on Euclidean distances to obstacles and other pedestrians. Alternative formulations assume elliptical (Johansson et al., 2007; Shukla, 2010), velocity-dependent (Chraibi et al., 2010) or predicted (Zanlungo et al., 2011) force fields. Validations against empirical data have been performed by Chraibi et al. (2010) for unidirectional flows and by Zanlungo et al. (2011) for crossing pedestrian streams. Lane formation and oscillations in bottlenecks can be reproduced by these models given low or medium densities. Köster et al. (2013) discuss numerical problems arising in social force models for higher densities.

1.4. Empirical studies of bidirectional pedestrian flows

Isobe et al. (2004) compare an extended version of the CA model of Tajima et al. (2002) with experimental data. The CA model reproduces flows and velocities of bidirectional pedestrian experiments with a 50/50 directional flow split around an average density of 2.5 pedestrians per square meter in a channel. Similar experiments are performed by Nagai et al. (2005) for exceptional walking situations (e.g. evacuations during earth quakes or fire evacuations).

Cheung and Lam (1997) study bidirectional pedestrian flows in the Hong Kong Mass Transit Railway. Focusing on the effect of the directional distribution of pedestrian flow, they observe that capacity and speed of the minority stream decrease with increasing majority stream. Lam et al. (2002, 2003) study bidirectional pedestrian flows in in- and outdoor walkways and estimate a modified BPR function (Bureau of Public Roads, 1964) that captures the effect of counter-flow through a flow-composition dependent capacity parameter. Helbing et al. (2005); Kretz et al. (2006) support the hypothesis that flow composition matters. They conduct bidirectional flow experiments with various flow compositions and densities and find that the sum of directional flows in the bidirectional case is higher than in the unidirectional case for similar densities.

Wong et al. (2010) develop and estimate a bidirectional FD mapping direction-specific densities for different intersection angles onto direction-specific flows. Xie et al. (2013), Xie and Wong (2014) develop the model of Wong et al. (2010) further and introduce velocities as additional explanatory variables. The endogenous velocity variable cannot be isolated in their model, requiring numerical solution techniques. It should be noted that the FD developed in the present paper also starts

out from a specification with endogenous velocity, but here also a reformulation with flow (or velocity) depending only on densities (i.e. exogenous variables) is obtained. Contrary to the previous findings, Zhang and Seyfried (2014) describes a dataset collected with volunteers during a popular science event where no significant difference between flows crossing at a 90 and a 180 degree angle is identifiable.

Zhang (2012) provides and discusses a comprehensive summary of empirical evidence on bidirectional FDs, including own in-laboratory experiments. A key observation is that unidirectional FDs have a unique maximum and zero flows at jam density, whereas bidirectional FDs mapping total densities on total flows tend to level out at a flow plateau for high total densities. Zhang et al. (2011, 2012) conclude from in-laboratory experiments that the bidirectional FD is insensitive to *limited* variations in the flow composition around symmetric densities; this observation is in line with Older (1968); Fruin (1971); Pushkarev and Zupan (1975, p. 86) and Løvås (1994). This insensitivity is explained already by Older (1968); Pushkarev and Zupan (1975, p. 86) through the formation of lanes that limit obstructions in the bidirectional case. This, however, cannot be generalized to the full range of possible density compositions because unidirectional flow is a limiting case of bidirectional flow and for high densities a unidirectional FD is systematically different from a bidirectional FD.

1.5. Synthesis

The bidirectional pedestrian FDs to be found in the literature can be characterized in terms of the following two classes. (i) Simulation-based FDs, mostly obtained with CA simulation models. Even at a mild level of complexity, their mathematical description is limited to approximation results (Schadschneider, 1998). However, a very useful property is that their parameters are often defined in terms of readily interpretable microscopic interactions. (ii) General functional forms, sometimes borrowed from the vehicular context, fitted to empirical data. Since the authors are not aware of any functional forms that are derived from first principles (and hence may be valid for all density regimes), extrapolation beyond observed densities is an issue.

Available empirical findings indicate that a bidirectional pedestrian FD that applies to all possible density compositions needs to satisfy the following criteria: (i) Reproducing the single-peaked shape of a unidirectional FD if one density vanishes, (ii) maintaining substantial flow levels in the balanced bidirectional case even for high densities, (iii) interpolating between unidirectional and balanced bidirectional flow based on principles rooted in pedestrian interactions.

This article derives such an FD in the form of a minimal closed-form specification.

The concrete approach taken is to first specify an utmost simple CA of the bidirectional flow process and to then analytically derive the corresponding bidirectional FD. The resulting FD relies on a minimal set of readily interpretable parameters (maximum walking speed, jam density, a collision avoidance parameter). It covers the entire density range in that it provides for all possible bidirectional density configurations separate flow rates in either direction. The proposed FD guarantees non-negative and bounded flows. Further, these flows can only lead to densities between zero and jam density. The mapping from parameters on flows is continuous; the mapping from densities on flows is continuous at least for strictly positive densities or for wide channels. The FD maintains these properties when its parameters are made density-dependent, providing a basic structure from which a wealth of alternative specifications can be derived. For density-independent parameters, the unidirectional projections of the FD are triangular. The proposed FD is verified by comparison to a widely accepted microscopic simulation model, and it is validated against an empirical dataset and a variety of empirical phenomena described in the literature. A very good fit against the data is obtained.

The remainder of this work is organized as follows. Section 2 introduces the proposed model and derives its properties. Experimental results are presented in Section 3. Finally, Section 4 summarizes and concludes the article.

2. Model specification and properties

The new bidirectional FD is developed as follows. First, a bidirectional CA is defined in Section 2.1. The stationary behavior of this model is then derived and analyzed in terms of a continuum approximation in Sections 2.2 and 2.3. Further properties of the model are developed in Sections 2.4 and 2.5.

2.1. Cellular automaton

A long homogenous channel is considered. Space is longitudinally discretized into cells of length L, which corresponds to the length of a standing pedestrian. The channel width is set to one pedestrian width; this assumption is relaxed later on. Two types of pedestrians are considered. Pedestrians of class 1 traverse the channel in one direction, pedestrians of class 2 traverse it in the opposite direction. The movement of a pedestrian in either class is guided by the following set of rules.

Rule 1 (Free flow speed limit): Let $\hat{v}$ be the maximum pedestrian velocity. A pedestrian stays at least $L/\hat{v}$ time units in a cell before advancing to the next cell.

Rule 2 (Minimum time gap): Let z be the minimum time gap between two pedestrians of the same class. A pedestrian enters a cell not earlier than z time units after the previous pedestrian of the same class has left that cell.

Rule 3 (Conflict delay): When two pedestrians from different classes face each other, they experience an additional delay D before switching places at free flow speed $\hat{v}$, meaning that the overall conflict resolution time is $D + L/\hat{v}$.

The first two rules correspond to the cellular automaton model CA(M) of Daganzo (2006), which produces vehicle dynamics that are consistent with the KWM, given a triangular fundamental diagram with free flow speed $\hat{v}$, jam density $\hat{\varrho} = 1/L$, and backward wave speed $L/z = 1/\hat{\varrho}z$. The third rule is the sole phenomenological addition proposed in this work. It provides a single-parameter approximation of how much two pedestrians get delayed in a conflict situation before they move past each other. This movement past each other is subsequently referred to as a "swap".

One may argue that a unidirectional FD originally derived for car traffic may be an inadequate starting point for a bidirectional pedestrian flow model. However, the flow is in either case controlled by humans with essentially identical objectives (making progress, avoiding crashes). It hence is plausible to assume the same underlying model structure and to make the difference, which is more in terms of physical capabilities and collision consequences, concrete in terms of different parameter values (see also Goffman (1971, pp. 6–7)). The challenge then becomes to capture mixed bidirectional flow, which does not exist in the vehicular context.

A behaviorally meaningful parametrization of this CA requires

$$\frac{1}{\hat{v}\hat{\varrho}} + D \;\geqslant\; z. \tag{1}$$

This means that the time it takes to advance by one cell through a conflict must not be smaller than the time it takes to advance by one cell while following a lead pedestrian. To justify (1), the following configuration is considered:

$t < 0$	∘	∘		•
$t = 0$	∘		∘	•

(2)

Here and in all subsequent figures of this type, the ∘-pedestrians move from left to right and the •-pedestrians move from right to left. The first column indicates the time at which the configuration is observed for the first time. At time $t = 0$, the leading ∘-pedestrian advances by one cell, entering into a conflict situation with the •-pedestrian on the right-hand side. Two continuations of this configuration are possible. If (1) did not hold, then the conflict would get resolved before the left-hand side ∘-pedestrian catches up, leading to the following configuration:

$t = D + 1/\hat{v}\hat{\varrho}$	∘		•	∘

(3)

This would mean that the left-hand side ∘-pedestrian continues to implement a time gap of duration $z > D + 1/\hat{v}\hat{\varrho}$ to its leader (now on the very right-hand side), even though a •-counter-flow pedestrian now separates the two ∘-pedestrians. As this is not considered sensible, $z \leqslant D + 1/\hat{v}\hat{\varrho}$ is assumed instead, implying the following, plausible continuation of the $t = 0$ configuration:

$t = z$		∘	∘	•

(4)

Based on these arguments, (1) is from now on postulated.

2.2. Specification of fundamental diagram

The previously specified CA is analyzed in terms of a continuum model FD. For this, large spatial scales are assumed, allowing to neglect the discrete nature of the pedestrian flow. The FD is derived based on the assumption that flow is maximized subject to given constraints (Ansorge, 1990), of which three types are identified.

1. The advancement of a pedestrian is bound by the maximum velocity $\hat{v}$ and further reduced by the conflict delay D.
2. Counter-flow pedestrians act as moving bottlenecks.
3. If the density in a given class is over-critical (i.e., congested), then the pedestrians in this class enter a follow-the-leader regime, implementing a time gap z.

Maintaining the symmetry with a class of existing FD specifications (Daganzo, 1994; Lebacque, 1996), these constraints are formulated in terms of a *counter-flow constrained sending function* and *a counter-flow constrained receiving function*. In the following, the constraints taking effect on pedestrian class $i \in \{1, 2\}$ are developed, with the respective other class (constituting the counter-flow) being denoted by $j \in \{1, 2\} \setminus \{i\}$.

The density ϱ_i of the pedestrians moving in direction i and the flow q_i in direction i are defined on a one-pedestrian-wide longitudinal section of the channel. This leads to the unit [pedestrians per meter] and [pedestrians per second] for (maximum) density and flow, which is convenient when drawing parallels to the single-lane CA. Flow, density, and velocity are coupled through

$$q_i = \varrho_i v_i. \tag{5}$$

The constraint (1) is subsequently respected. Further, densities are assumed to comply with

$$\varrho_i > 0 \tag{6}$$

$$\varrho_i + \varrho_j \leqslant \hat{\varrho}. \tag{7}$$

The case of strictly zero densities is discussed separately further below. Formulations for channels that are wider than one pedestrian are also given later in the text.

2.2.1. Counter-flow constrained sending function

Given that a class-i pedestrian is not constrained by a leading pedestrian of its own class, its advancement is defined by the free-flow speed limit $\hat{v}$ and the experienced conflict delay. This conflict delay depends on how much counter-flow is present. Specifically, the time rate at which a class-i pedestrian experiences conflicts is $(v_i + v_j)\varrho_j$ (in conflicts per time unit). Since the time it takes a class-i pedestrian to advance by a distance of $1/\varrho_i$ is $1/\varrho_i v_i = 1/q_i$, the number of conflicts a class-i pedestrian encounters when advancing by $1/\varrho_i$ is $(v_i + v_j)\varrho_j/q_i$. In consequence, the time $1/q_i$ it takes a class-i pedestrian to advance by $1/\varrho_i$ at speed v_i follows

$$\frac{1}{q_i} \quad \geqslant \quad \frac{1}{\varrho_i \hat{v}} + D\frac{(v_i + v_j)\varrho_j}{q_i}, \tag{8}$$

where the first addend on the right-hand side represents the free flow travel time, the second addend represents the additional delay incurred by the counter-flow, and an inequality is written to account for the possibility of other more stringent causes of delay, as discussed further below. Solving for q_i yields

$$q_i \ \leqslant \ S(\varrho_i, \varrho_j, q_j) \tag{9}$$

with

$$S(\varrho_i, \varrho_j, q_j) = \varrho_i \hat{v}\frac{1 - Dq_j}{1 + D\hat{v}\varrho_j} \tag{10}$$

being the *counter-flow constrained sending function*. It decreases both with the counter-flow rate q_j and the counter-flow density ϱ_j. [1]

2.2.2. Counter-flow constrained receiving function

A class-j pedestrian constitutes from the perspective of class i a moving bottleneck with flow capacity

$$B = \left(D + \frac{1}{\hat{v}\hat{\varrho}}\right)^{-1} \tag{11}$$

$$= \frac{\hat{v}\hat{\varrho}}{1 + D\hat{v}\hat{\varrho}}. \tag{12}$$

This results from the fact that a hypothetical *standing* counter-flow pedestrian (i.e. one that does not advance when performing a swap) leaves one pedestrian through per $D + \frac{1}{\hat{v}\hat{\varrho}}$ time units. Constraining the class-i flow because of this bottleneck effect of the class-j flow corresponds to

$$(v_i + v_j)\varrho_i \ \leqslant \ \frac{\hat{v}\hat{\varrho}}{1 + D\hat{v}\hat{\varrho}}. \tag{13}$$

Solving for q_i yields

$$q_i \ \leqslant \ R(\varrho_i, \varrho_j, q_j) \tag{14}$$

with

$$R(\varrho_i, \varrho_j, q_j) = \frac{\hat{v}\hat{\varrho}}{1 + D\hat{v}\hat{\varrho}} - \frac{q_j\varrho_i}{\varrho_j} \tag{15}$$

being (the first part of) the *counter-flow constrained receiving function*. It decreases with the counter-flow velocity $v_j = q_j/\varrho_j$ and with class i's density ϱ_i. Recall that for now only strictly positive densities are considered.

The congested branch of a unidirectional triangular fundamental diagram further prescribes

$$q_i \ \leqslant \ K(\varrho_i) \tag{16}$$

[1] To obtain a proper sending function in the sense of Daganzo (1994), Lebacque (1996), one would also have to truncate S at the (yet to be developed) fundamental diagram's capacity.

with

$$K(\varrho_i) \;=\; \frac{1}{z\hat{\varrho}}(\hat{\varrho}-\varrho_i) \tag{17}$$

being the (the second part of) the *counter-flow constrained receiving function.*

2.2.3. First instance of the fundamental diagram

An FD is obtained when both flows q_i and q_j are maximized subject to all sending and receiving constraints. This corresponds to a solution of the following system of equations:

$$q_i = \min\left\{S(\varrho_i,\varrho_j,q_j),\, R(\varrho_i,\varrho_j,q_j),\, K(\varrho_i)\right\} \quad \forall (i,j)\in\{(1,2),(2,1)\} \tag{18}$$

where S, R, and K are defined in (10), (15), (17). Since all involved functions are continuous, the implicit function theorem ensures that the flow solutions of this model depend continuously on densities and model parameters.

2.3. Analysis of fundamental diagram

A closed-form expression of the model (18) is subsequently derived and its relevant properties are established.

2.3.1. Closed-form solutions for relevant congestion regimes

In the *SS congestion regime*, either flow is constrained by its sending function: $q_i^{\mathrm{SS}} = S(\varrho_i,\varrho_j,q_j^{\mathrm{SS}})$ and $q_j^{\mathrm{SS}} = S(\varrho_j,\varrho_i,q_i^{\mathrm{SS}})$. Inserting (10) and solving for the flows yields

$$q_i^{\mathrm{SS}} = \varrho_i\hat{v}\frac{1+D\hat{v}(\varrho_i-\varrho_j)}{1+D\hat{v}(\varrho_i+\varrho_j)} \tag{19}$$

$$q_j^{\mathrm{SS}} = \varrho_j\hat{v}\frac{1+D\hat{v}(\varrho_j-\varrho_i)}{1+D\hat{v}(\varrho_i+\varrho_j)}. \tag{20}$$

In the *SR congestion regime*, flow i is constrained by its sending function and flow j is constrained by (the first part of) its receiving function: $q_i^{\mathrm{SR}} = S(\varrho_i,\varrho_j,q_j^{\mathrm{SR}})$ and $q_j^{\mathrm{SR}} = R(\varrho_j,\varrho_i,q_i^{\mathrm{SR}})$. Inserting (10) and (15) and solving for the flows yields

$$q_i^{\mathrm{SR}} = \frac{\hat{v}\varrho_i}{1+D\hat{v}\hat{\varrho}} \tag{21}$$

$$q_j^{\mathrm{SR}} = \frac{\hat{v}(\hat{\varrho}-\varrho_j)}{1+D\hat{v}\hat{\varrho}}. \tag{22}$$

Symmetrically, the flows in the *RS configuration* result from exchanging the i and j index.

The *SS configuration* is delineated in the (ϱ_i,ϱ_j) plane against the *RS configuration* and the *SR configuration* by the inequalities

$$q_i^{\mathrm{SS}} \;=\; S(\varrho_i,\varrho_j,q_j^{\mathrm{SS}}) \;\leqslant\; R(\varrho_i,\varrho_j,q_j^{\mathrm{SS}}) \tag{23}$$

$$q_j^{\mathrm{SS}} \;=\; S(\varrho_j,\varrho_i,q_i^{\mathrm{SS}}) \;\leqslant\; R(\varrho_j,\varrho_i,q_i^{\mathrm{SS}}). \tag{24}$$

Inserting (15), (19), (20) and rearranging leads to

$$\varrho_j \;\geqslant\; \varrho_i\frac{2+D\hat{v}\hat{\varrho}}{D\hat{v}\hat{\varrho}} - \frac{1}{D\hat{v}} \tag{25}$$

$$\varrho_j \;\leqslant\; \varrho_i\frac{D\hat{v}\hat{\varrho}}{2+D\hat{v}\hat{\varrho}} + \frac{\hat{\varrho}}{2+D\hat{v}\hat{\varrho}}, \tag{26}$$

respectively. The two separating lines have both a positive slope in the (ϱ_i,ϱ_j) plane and intersect at $\varrho_i=\varrho_j=\hat{\varrho}/2$. They are indicated in Fig. 1.

Proposition 1. *Given strictly positive densities complying with (7) and parameters complying with (1), the model is fully specified through the SS, RS, and SR configuration.*

Proof. In the *RR configuration*, the flows are defined through $q_i^{\mathrm{RR}} = R(\varrho_i,\varrho_j,q_j^{\mathrm{RR}})$ and $q_j^{\mathrm{RR}} = R(\varrho_j,\varrho_i,q_i^{\mathrm{RR}})$. Inserting (15) and solving for the flows leads to

$$\varrho_i=\varrho_j \;\Rightarrow\; q_i^{\mathrm{RR}}+q_j^{\mathrm{RR}} = \frac{\hat{v}\hat{\varrho}}{1+D\hat{v}\hat{\varrho}} \tag{27}$$

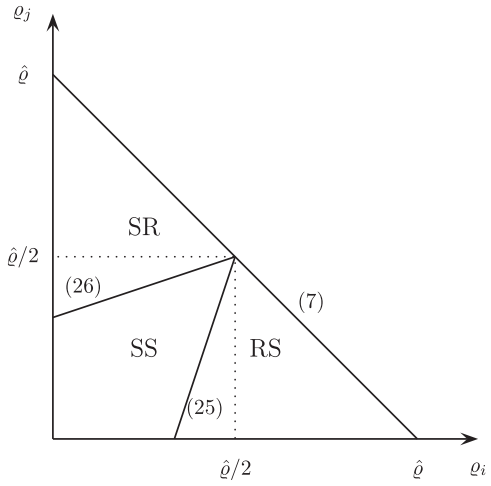

Fig. 1. Density regions of relevant congestion configurations.

and no solution otherwise. If there were densities $(\varrho_i, \varrho_j) = (\varrho, \varrho)$ where the RR configuration took effect, $q_i^{\mathrm{RR}} + q_j^{\mathrm{RR}} = R(\varrho, \varrho, q_j^{\mathrm{RR}}) + R(\varrho, \varrho, q_i^{\mathrm{RR}}) < S(\varrho, \varrho, q_j^{\mathrm{RR}}) + S(\varrho, \varrho, q_i^{\mathrm{RR}})$ would have to hold. (The case of strict equality can be ignored due to the continuity of the model.) However, inserting (10) and (27) into this expression leads to $\varrho > \hat{\varrho}/2$, which contradicts (7).

The *KS configuration* taking effect requires $q_i^{\mathrm{KS}} = K(\varrho_i) < R(\varrho_i, \varrho_j, q_j^{\mathrm{KS}})$ with $q_j^{\mathrm{KS}} = S(\varrho_j, \varrho_i, q_i^{\mathrm{KS}})$. Substituting (10), (15), (17) and rearranging yields $1/\hat{v}\hat{\varrho} + D < z$, which contradicts (1). Symmetrically for the *SK configuration*.

The *KR configuration* taking effect requires $q_i^{\mathrm{KR}} = K(\varrho_i) < R(\varrho_i, \varrho_j, q_j^{\mathrm{KR}})$ and $K(\varrho_i) < S(\varrho_i, \varrho_j, q_j^{\mathrm{KR}})$, both with $q_j^{\mathrm{KR}} = R(\varrho_j, \varrho_i, q_i^{\mathrm{KR}})$. Substituting (10), (15), (17) and rearranging yields $\varrho_i < \varrho_j$ from the first requirement and $(\hat{\varrho} - \varrho_i)(1/\hat{v}\hat{\varrho} + D) < z\varrho_i$ from the second requirement. Combining these expressions and using $\varrho_j \leqslant \hat{\varrho} - \varrho_i$ leads to $1/\hat{v}\hat{\varrho} + D < z$, which contradicts (1). Symmetrically for the *RK configuration*.

The *KK configuration* taking effect requires $q_i^{\mathrm{KK}} = K(\varrho_i) < R(\varrho_i, \varrho_j, q_j^{\mathrm{KK}})$ and $q_j^{\mathrm{KK}} = K(\varrho_j) < R(\varrho_j, \varrho_i, q_i^{\mathrm{KK}})$. Inserting (15), (17), (1) and evaluating results in both $\varrho_i > \hat{\varrho}/2$ and $\varrho_j > \hat{\varrho}/2$, which contradicts (7).

This excludes all configurations but SS, RS, SR from consideration. □

The model (18) hence simplifies into

$$q_i = \min\left\{S(\varrho_i, \varrho_j, q_j), R(\varrho_i, \varrho_j, q_j)\right\} \quad \forall (i,j) \in \{(1,2),(2,1)\} \tag{28}$$

with S and R defined in (10) and (15). A closed form of the model for $\varrho_i \in (0, \hat{\varrho}]$ and $\varrho_j \in (0, \varrho_i]$ (sufficient due to its symmetry) reads as follows:

$$\begin{pmatrix} q_i \\ q_j \end{pmatrix} = \mathrm{FD}(\varrho_i, \varrho_j) = \begin{cases} \frac{\hat{v}}{1+D\hat{v}(\varrho_i+\varrho_j)} \begin{pmatrix} \varrho_i[1+D\hat{v}(\varrho_i - \varrho_j)] \\ \varrho_j[1+D\hat{v}(\varrho_j - \varrho_i)] \end{pmatrix} & \text{if} \varrho_j \geqslant \varrho_i \frac{2+D\hat{v}\hat{\varrho}}{D\hat{v}\hat{\varrho}} - \frac{1}{D\hat{v}} \text{(SS regime)} \\ \frac{\hat{v}}{1+D\hat{v}\hat{\varrho}} \begin{pmatrix} \hat{\varrho} - \varrho_i \\ \varrho_j \end{pmatrix} & \text{otherwise (RS regime).} \end{cases} \tag{29}$$

The following model properties can be immediately derived from (29):

- The flows depend continuously on densities and parameters.
- The model has one and only one solution for each feasible density and parameter configuration.
- The flows are non-negative.
- Negative densities cannot be attained.
- The jam density cannot be exceeded.

The third last property holds for all equations because of the respective density range specifications. The second last property results from the fact that for a zero density the respective flow becomes zero. The last property is shown by reading the implication $(\varrho_i + \varrho_j = \hat{\varrho}) \Rightarrow (q_i = q_j)$ out of the second case of (29): For a unidirectional model, one would have to show $(\varrho_i = \hat{\varrho}) \Rightarrow (q_i = 0)$. The bidirectional model, however, allows even in complete congestion for some flow due to conflicting pedestrians switching places. As long as this exchange flow is symmetric, the jam density is not exceeded. Regarding the last property, it should be acknowledged that the present analysis considers stationary conditions only. Appert-Rolland et al.

(2014) present an approach that reflects the difficulty of ensuring this constraint in the context of a bidirectional flow model with second-order dynamics.

The unidirectional backward wave speed $1/\hat{\varrho}z$ does not enter (29), where its bidirectional counterpart is $\hat{v}/(1+D\hat{v}\hat{\varrho})$. The FD would therefore behave discontinuously when going from an arbitrarily small but strictly positive counter-flow density to a unidirectional FD corresponding to a strictly zero counter-flow density. This discontinuity vanishes only if

$$z = \frac{1}{\hat{v}\hat{\varrho}} + D. \tag{30}$$

The validity of the *continuity constraint* (30) will therefore be investigated both conceptually and empirically in the following. It should be clarified upfront, however, that the continuity constraint (30) is an additional modeling assumption, and as such it may be dropped if empirical or other evidence does not support this assumption. Removing the continuity constraint (30) leaves the proposed bidirectional FD (29) completely intact, only that then a discontinuity in the case of vanishing counter-flow is allowed for.

2.4. Discussion of continuity constraint

The counter-flow constrained sending function (10) converges for vanishing counter-flow continuously to the uncongested branch of a unidirectional triangular FD with $q_i = \hat{v}\varrho_i$. The continuity constraint (30) is hence only relevant in the RS and the SR regime. Relying on the proposed FD's symmetry, only the RS regime is subsequently considered, meaning that $\varrho_i > \varrho_j$ is assumed without loss of generality, cf. Fig. 1. Adopting the CA perspective, there hence are on average ϱ_i/ϱ_j class-i pedestrians between two class-j pedestrians. The class-j pedestrians affect in the RS regime the class-i pedestrians as moving bottlenecks. Given a single-lane channel, the class-i density profile between two class-j pedestrians is hence split into two regions, an upstream free-flowing region and a downstream queueing region:

⋯				○	○	○	●				○	○	○	●	⋯

(31)

where ○ represents class-i pedestrians moving from left to right and ● represents class-j pedestrians moving from right to left. A share of the ○-pedestrians queues up in front of the ●-moving bottlenecks. The remaining ○-pedestrians, which have just moved through a ●-bottleneck but have not yet reached the ○-queue in front of the next ●-bottleneck, are freely flowing; instances of these are not drawn in order to keep the figure simple.

Now a channel that is wider than one pedestrian is considered. Since densities and flows in (29) are defined for channels that are one pedestrian wide, cf. Section 2.2, this model can technically be carried over to wider channels by making the implicit assumption that a wide channel functions like several independent narrow channels in parallel. In CA terms, this would lead to the following picture of a multi-channel RS regime:

⋯	○	○	●				○	○	○	●				○	⋯
⋯				○	○	○	●				○	○	○	●	⋯
⋯	○	○	○	●				○	○	○	●				⋯

(32)

The assumption of independent channels implies the assumption of implausible queues where ○-pedestrians that queue in front of a ●-moving bottleneck do not make use of the space available in adjacent channels; lateral movement is not included in the model.

A situation where the ○-pedestrians also spread out laterally until the available space is homogeneously used would, on the other hand, look as follows:

⋯		○	●		○		○		○	●		○		○	⋯
⋯		○		○		○	●		○		○		○	●	⋯
⋯	○		○	●		○		○		○	●		○		⋯

(33)

Comparing (32) and (33), one observes that the inclusion of lateral movement in the model has the same effect as a density reduction in the ○-queues until these queues stretch over the entire space between two ●-pedestrians. Observing that there is no counter-flow *within* the ○-queue, the flow in that stretched queue follows the congested branch of a unidirectional triangular fundamental diagram with backward wave speed $1/\hat{\varrho}z$:

$$q_i = \frac{1}{\hat{\varrho}z}(\hat{\varrho} - \varrho_i). \tag{34}$$

Equating (34) with the class-i flow defined for the RS regime in (29) then again leads to an expression that is identical to the continuity constraint (30). This holds of course only for channels that are wide enough to allow for lateral movements.

Intuitively: Using the continuity constraint (30) to compute a conflict delay parameter D from a given time gap z and a given maximum density $\hat{\varrho}$ has the same effect as assuming that the conflict resolution time is minimized by lateral pedestrian movements. This minimization can be read out of the fundamental assumption (1), where compliance with

the continuity constraint (30) means that the D parameter attains its lower bound. This in turn is equivalent to postulating that pedestrians perform lateral movements such that their flow is maximized, which is completely in line with the flow-maximization principle of Ansorge (1990).

2.5. Capacity flows

For a given class-j flow q_j and density ϱ_j, the class-i flow can be written in the form of a unidirectional FD

$$q_i = \min\left\{\hat{v}(q_j,\varrho_j)\cdot\varrho_i,\, w(q_j,\varrho_j)\cdot(\hat{\varrho}(q_j,\varrho_j)-\varrho_i)\right\} \tag{35}$$

with counter-flow dependent parameters

$$\hat{v}(q_j,\varrho_j) = \hat{v}\frac{1-Dq_j}{1+D\hat{v}\varrho_j} \tag{36}$$

$$w(q_j,\varrho_j) = \frac{q_j}{\varrho_j} = v_j \tag{37}$$

$$\hat{\varrho}(q_j,\varrho_j) = \frac{\hat{v}\hat{\varrho}}{1+D\hat{v}\hat{\varrho}}\cdot\frac{\varrho_j}{q_j}, \tag{38}$$

cf. (10) and (15). Assuming both pedestrian classes to attain their capacity flows q_i^* and q_j^*, one obtains, by equating the flow of the uncongested and the congested branch of (35), the critical density

$$\varrho_i^* = \frac{w(q_j^*,\varrho_j^*)}{\hat{v}(q_j^*,\varrho_j^*)+w(q_j^*,\varrho_j^*)}\cdot\hat{\varrho}(q_j^*,\varrho_j^*). \tag{39}$$

Inserting (36)–(38) and noting in (35) that $\hat{v}(q_i^*,\varrho_i^*) = q_j^*/\varrho_j^*$, this becomes

$$\varrho_i^* = \frac{1}{\hat{v}(q_j^*,\varrho_j^*)+\hat{v}(q_i^*,\varrho_i^*)}\cdot\frac{\hat{v}\hat{\varrho}}{1+D\hat{v}\hat{\varrho}}, \tag{40}$$

implying $\varrho_i^* = \varrho_j^* = \varrho^*$ and, by symmetry of the FD, $q_i^* = q_j^* = q^*$. Inserting this into (40) and using $q^* = \hat{v}(q^*,\varrho^*)\varrho^*$ leads to the following capacity flow for each direction:

$$q^* = \frac{1}{2}\cdot\frac{\hat{v}\hat{\varrho}}{1+D\hat{v}\hat{\varrho}}. \tag{41}$$

Since the point $(\varrho_i,\varrho_j) = (\varrho^*,\varrho^*)$ is located in the SS regime, cf. Fig. 1, one further has

$$q^* = S(\varrho^*,\varrho^*,q^*) \tag{42}$$

which, when inserting (10) and (41) and rearranging results in the critical density

$$\varrho^* = \frac{\hat{\varrho}}{2}. \tag{43}$$

This means, intuitively, that if two large groups of otherwise unobstructed pedestrians moving in opposite directions meet at an interface, e.g., a wide open door between two rooms, then (i) the average density at the interface becomes maximal, (ii) the space within the interface is on average equally shared between both groups, and (iii) the average throughput of the interface in either direction is given by (41).

When comparing this result further below to empirical findings, it should be noted that empirical densities at capacity flows are fluctuating. These fluctuations are likely to be stronger down- than upwards because of the increasing pressure working against densities beyond jam density. That is, the observed average densities at bidirectional capacity flows are likely to be somewhat below (43). It should also be kept in mind that these results are obtained under the assumption that no further boundary constraints affect the flows.

3. Experiments

The first experiment in Section 3.1 verifies the proposed bidirectional FD by comparison to synthetic data from a pedestrian micro-simulation. The second experiment in Section 3.2 validates the FD against a real data set. The last Section 3.3 explains a number of further empirical findings from the literature in terms of the proposed FD.

Most pedestrian data in the literature is given in terms of "specific" densities and flows that have units [pedestrians per area] and [pedestrians per time unit per cross-section-width], respectively. The proposed FD is defined in terms of densities ϱ and flows q that have units [pedestrians per length unit] and [pedestrians per time unit] and apply to a channel that is as

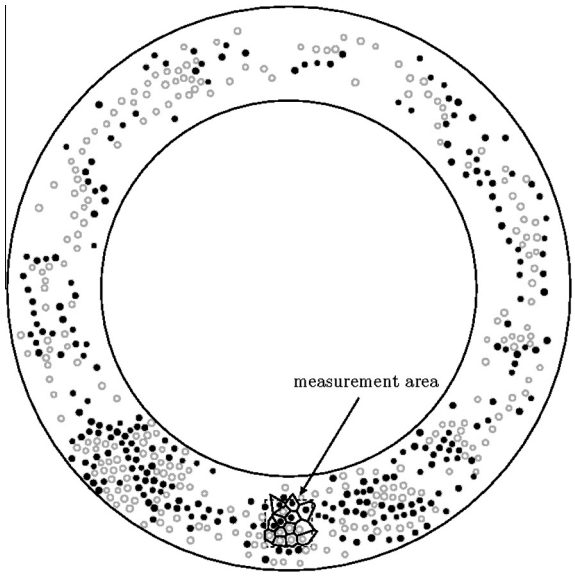

Fig. 2. Illustration of the ring road experiment. There are two groups of simulated pedestrians. Group one indicated by ∘ moves clockwise and group two indicated by • moves counter-clockwise.

wide as one pedestrian. Denoting specific densities and flows from now on by $\tilde{\varrho}$ and $\tilde{q}$ and letting the width of a pedestrian be b, the following relationships hold:

$$\varrho = b\tilde{\varrho} \tag{44}$$

$$q = b\tilde{q}. \tag{45}$$

The following conventions are therefore adopted: (i) All data is presented in terms of specific densities $\tilde{\varrho}$ and flows $\tilde{q}$. (ii) Whenever specific densities or flows need to be inserted into any of the previously developed mathematical expressions, they are first normalized to one channel width by using (44) and (45). The pedestrian width b is subsequently set to $24\prime\prime = 0.61\,\text{m}$, following Fruin (1971, p.67).

3.1. Comparison to the social force model

The social force model is the arguably most widely known microscopic simulation model of pedestrian dynamics on arbitrary topologies (Helbing and Molnár, 1995; Helbing et al., 2000). The objective of this experiment is to compare the proposed bidirectional FD to the empirical FD produced by the social force model. For this, bidirectional flows are simulated with the social force model on a ring road of 30 m diameter and 10 m width. An illustration is given in Fig. 2.

Flows and densities are measured in a 5 m×5 m area as shown in Fig. 2, following Steffen and Seyfried (2010). In each simulation time step, a Voronoi diagram is computed, with each pedestrian in the measurement region constituting the center of one Voronoi cell.[2] The specific density in the measurement area is the number of pedestrians divided by the sum of all Voronoi cell areas. This leads to lower measurement scatter than dividing the number of pedestrians by the measurement area size because the Voronoi cells capture more precisely the effectively occupied space by pedestrians at the boundaries of the measurement area. Zhang et al. (2011) discuss this measurement technique in greater detail. The speed of a pedestrian in longitudinal corridor direction can be directly extracted from the social force model. The space-mean speed in the measurement region is the average of all individual speeds weighted by the area of the respective Voronoi cells. Here again, the Voronoi method yields less scatter than simply averaging over all pedestrians. The instantaneous specific flow in the measurement region is computed as the product of specific density and space-mean speed. Direction-specific quantities are computed by considering only those pedestrians that were a priori assigned to the respective direction.

The genuine social force model of Helbing et al. (2000) is used, also deploying identical parameters. The continuous-time model is solved with the Euler method in 0.1 s time steps. Nine simulation runs are conducted. In each run, 2000 pedestrians walk along the ring road for overall 80 simulation minutes. The pedestrians are split into two groups. Group one walks in clockwise direction and group two walks in counter-clockwise direction. The share of group-one pedestrians is varied from 10% to 90% in 10%-steps from run to run, with the respective remainder of the pedestrians being assigned to group two.

Each simulation is run through a warm-up period of ten minutes until stationarity is postulated and simulated measurements are extracted. The empirical FD resulting from all simulated data points is shown in Fig. 3(a). It displays the specific

[2] A Voronoi cell is defined as the set of all points that are closer to that cell's center than to all other cell centers.

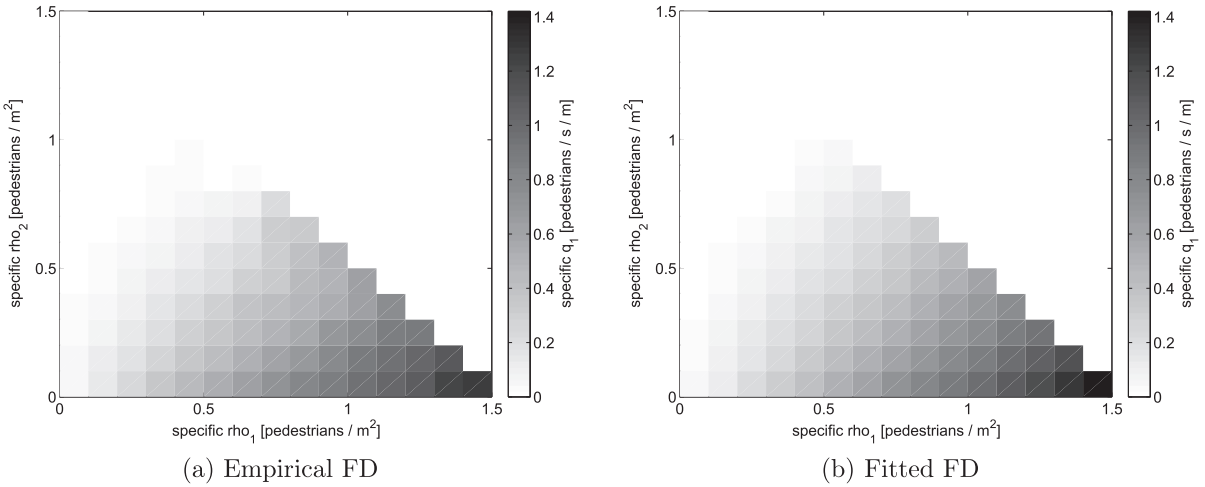

Fig. 3. Fit against the social force model. Displayed are specific flows in pedestrians per second per cross-section-meter. Darker shadings indicate higher flows.

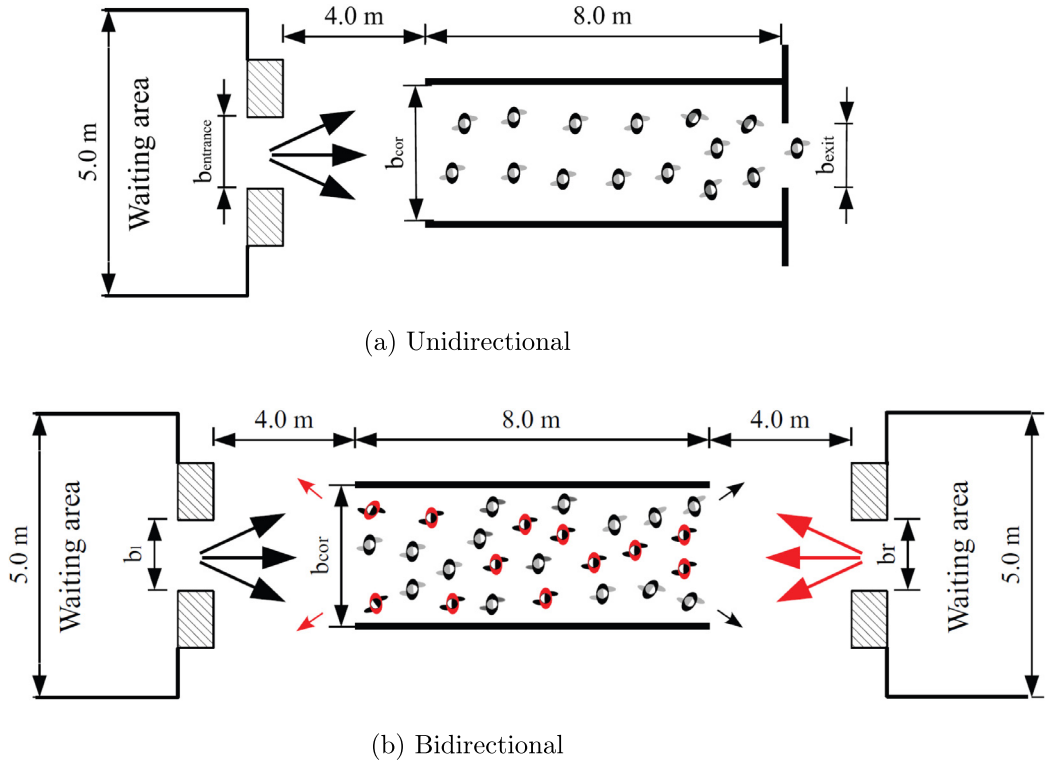

Fig. 4. Layout of real data collection (Zhang, 2012).

flow $\tilde{q}_i$ of one pedestrian group over its own specific density $\tilde{\varrho}_i$ on the x-axis and the specific counter-flow density $\tilde{\varrho}_j$ on the y-axis. All simulated data points $(\tilde{\varrho}_1, \tilde{\varrho}_2, \tilde{q}_1, \tilde{q}_2)$ enter this FD twice, once as $(\tilde{\varrho}_1, \tilde{\varrho}_2, \tilde{q}_1)$ and once as $(\tilde{\varrho}_2, \tilde{\varrho}_1, \tilde{q}_2)$. Apart from the feasibility of doing this in symmetric conditions, it eliminates possibly remaining biases due to the ring road's curvature. (No such bias could, however, be identified based on a visual inspection of the data.)

Due to the continuous variability of the traffic conditions in the measurement area, all density regimes up to a total specific density of 1.5 pedestrians per m^2 could be observed a large number of times. Higher total densities, however, turned out to be problematic to implement. They come with the earlier mentioned numerical difficulties in solving the social force model (Köster et al., 2013). A modified social force model allowing for higher densities was therefore implemented

(Helbing et al., 2005). This model, however, led to the formation of turbulent boundary regions between the two pedestrian groups. To the best of the authors' knowledge, no empirical support for such a phenomenon exists, rendering it questionable as a reference point for the newly proposed FD.

The omission of high densities allows exclusively for observations in the SS configuration. This can be concluded from a comparison of Fig. 3(a) with Fig. 1 and by reading out of (29) that transitions from SS to SR or RS come with a flow maximum along the coordinate axis. Hence, only the two parameters $\hat{v}$ and D appearing in the first case of the model (29) can be identified. An ordinary least squares estimation results in the parameter values $\hat{v} = 1.00\,\mathrm{m/s}, D = 2.69\,\mathrm{s}$, and a coefficient of determination of $R^2 = 0.90$. Arguably even more insightful is a comparison of the empirical and the estimated FD in Fig. 3(a) and (b), respectively. The structure of the empirical FD is captured very well by the proposed FD.

This experiment also led to the insight that the estimation of an FD is anything but a straightforward endeavor. First, the data is typically available in the form of time series, introducing serial correlation into the regression residuals and therefore calling for dedicated techniques when estimating a parameter covariance matrix. Second (and more severe), the dependent variables (flows) of one point in time enter the independent variables (densities) of later times, leading to correlations between residuals and explanatory variables (known as endogeneity), which requires careful correction to avoid biased parameter estimates. (Greene (2003) provides more background on these two issues.) Third, the spatial distribution of pedestrians in the social force model never attains homogeneity; Fig. 2 reveals both lane-formation and clustering. Fourth, the force-based simulation model allows for finite accelerations, such that even if the measurement region is uncongested pedestrians may not yet have reached their maximum velocity. (The experimental results confirm this in that the maximum velocity parameter in the social force model was indeed set to 1.34 m/s but estimated to be only 1.00 m/s.) This work does not attempt to resolve these statistical problems, which clearly deserve future attention. The presented experiments serve the sole purpose of demonstrating a meaningful *structure* of the proposed FD.

Comparing two models does of course not provide empirical evidence for one or the other model. It can, however, serve as a plausibility check. Here, the affirmative result was obtained that the proposed bidirectional FD is consistent with the FD that emerges of a widely accepted microscopic simulation model of pedestrian dynamics in the free-flow regime.

3.2. Calibration against real data

The data used here was collected under laboratory conditions by Zhang et al. (2011, 2012). It consists of a unidirectional dataset and a bidirectional dataset, labeled "U-300" and "BFR-DML-360" in Zhang (2012). The experimental layout is sketched in Fig. 4. On top, the collection of the unidirectional data is shown. Pedestrians enter an 8 m long and $b_{\mathrm{corr}} = 3\,\mathrm{m}$ wide channel from a waiting area through a bottleneck of b_{entrance} width. A bottleneck of width b_{exit} at the end of the channel allows to create congested conditions. Pedestrians who have left the channel walk around its outside and return to the waiting area. Fig. 4(b) shows the bidirectional data collection. Two groups of pedestrians enter a $b_{\mathrm{corr}} = 3.6\,\mathrm{m}$ wide channel from their respective waiting area on the left- and right-hand side. Once they have walked through the channel, they walk around its outside and return to their waiting area. The density within the channel is controlled by the width b_{r} of either waiting area's release, resulting in on average balanced densities in the channel. In this data set, only the total specific density and flow (summed over both directions) are documented. In both settings, the channel width b_{corr} serves as an additional degree of freedom. Flows and densities are extracted by video from a 2 m long cross-section in the center of the channel, using the same method as described in Section 3.1.

Let $(\tilde{\varrho}^r_{\mathrm{unidir}}, \tilde{q}^r_{\mathrm{unidir}})$ be the rth unidirectional specific (density, flow) data point, and let $(\tilde{\varrho}^r_{\mathrm{bidir}}, \tilde{q}^r_{\mathrm{bidir}})$ be the rth bidirectional data point consisting of total specific density and total specific flow. *One* bidirectional FD is fitted against *both* datasets. Given that the channel is much wider than one pedestrian, the continuity constraint is used, in that only the parameters $(\hat{v}, \hat{\varrho}, D)$ are estimated and the minimum time gap z is inferred from (30). The following ordinary least squares estimator is used:

$$\min_{(\hat{v},\hat{\varrho},D)} \sum_r \left(b\tilde{q}^r_{\mathrm{unidir}} - \mathrm{FD}_1\left(b\tilde{\varrho}^r_{\mathrm{unidir}}, 0\right)\right)^2 + \sum_r \left(\frac{b\tilde{q}^r_{\mathrm{bidir}}}{2} - \mathrm{FD}_1\left(\frac{b\tilde{\varrho}^r_{\mathrm{bidir}}}{2}, \frac{b\tilde{\varrho}^r_{\mathrm{bidir}}}{2}\right)\right)^2 \tag{46}$$

where $\mathrm{FD}_1(\varrho_1, \varrho_2)$ returns the prediction of the bidirectional FD (29) for q_1. The scaling with the pedestrian width $b = 0.61\,\mathrm{m}$ allows to insert specific densities into the FD and to compare its predictions to specific flows, as explained in the beginning of Section 3. The addends of the first sum evaluate the bidirectional FD effectively like a univariate FD and compare its prediction to the measured univariate flow. The addends of the second sum evaluate the bidirectional FD by splitting the total density half/half for each direction and comparing its prediction for one direction to half of the total measured flow; this approach is commented on further below.

Assuming a constant (density-independent) D parameter yields the estimated parameters $\hat{v} = 1.26\,\mathrm{m/s}, \hat{\varrho}/b = 5.09\,\mathrm{m}^{-2}$, $D = 0.45\,\mathrm{s}$ (implying $z = 0.60\,\mathrm{s}$) and leads to the data fit shown in Fig. 5(a) and (b). Dividing the maximum density $\hat{\varrho}$ by the pedestrian width b turns it into a specific maximum density. While the unidirectional projection of the FD captures the shape of the data cloud fairly correctly ($R^2 = 0.74$), the structure of the bidirectional data is not well represented ($R^2 = 0.52$). In particular, the flows for high densities are overestimated.

The following modified specification with a density-dependent D parameter (and by (30) an also density-dependent minimum time gap z) is hence adopted:

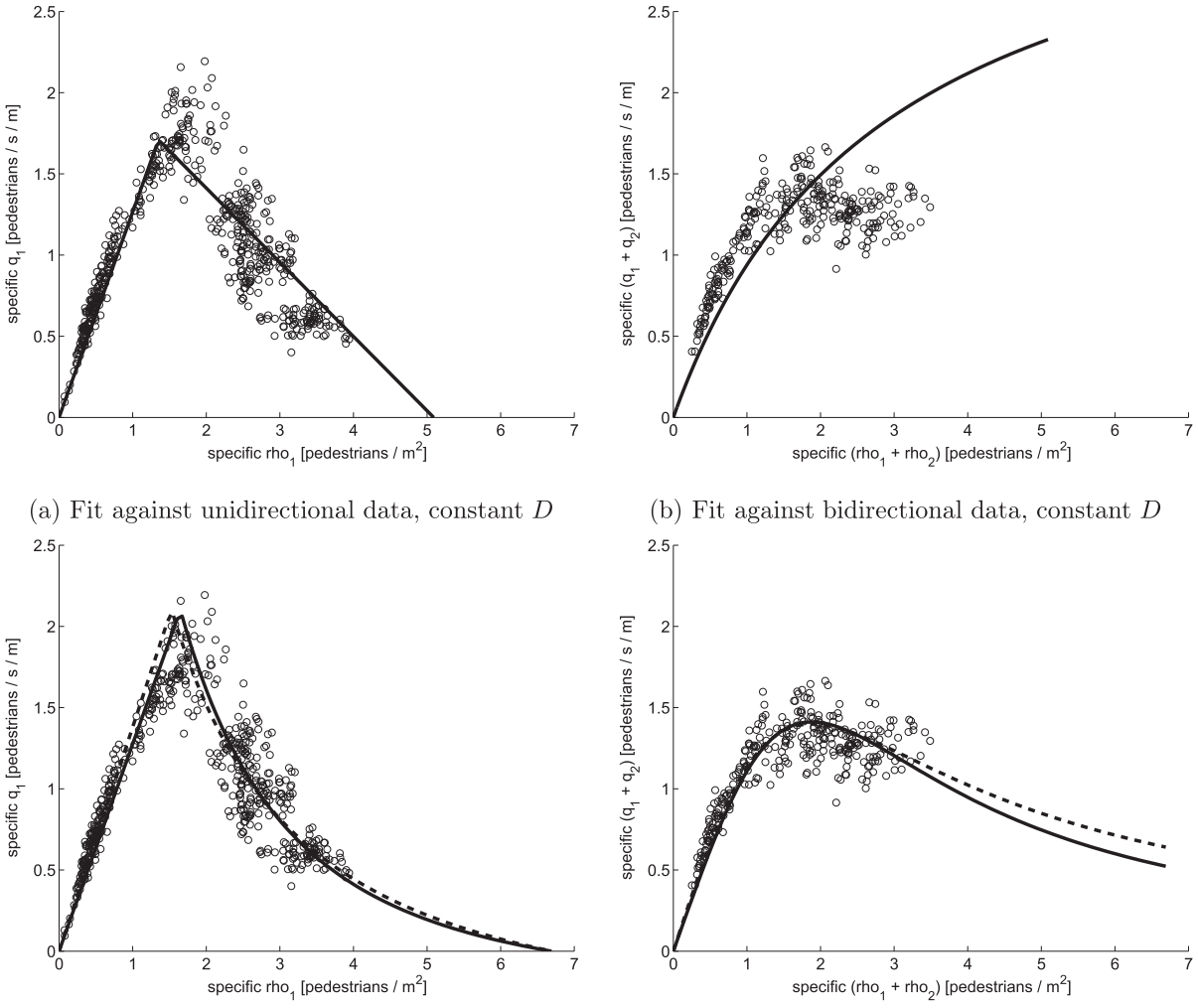

(a) Fit against unidirectional data, constant D

(b) Fit against bidirectional data, constant D

(c) Fit against unidirectional data, variable D

(d) Fit against bidirectional data, variable D

Fig. 5. Fit of FD into real data points.

$$D(\tilde{\varrho}_1, \tilde{\varrho}_2) = \alpha + \beta \left(\frac{b\tilde{\varrho}_1 + b\tilde{\varrho}_2}{1\,\mathrm{m}^{-1}} \right)^{\gamma} \tag{47}$$

with α, β, γ being additional parameters. The second addend aims at capturing increased friction (and hence conflict delay) at higher total densities. Estimating this model yields $\hat{v} = 1.27\,\mathrm{m/s}$, $\hat{\varrho}/b = 6.69\,\mathrm{m}^{-2}$, $(\alpha, \beta, \gamma) = (0.0\,\mathrm{s}, 0.39\,\mathrm{s}, 1.43)$ and the data fit represented by the solid lines in Fig. 5(c) and (d). Not only the bidirectional flow is now well described by the model ($R^2 = 0.79$),also the fit to the unidirectional data has clearly improved ($R^2 = 0.85$). One also observes how the relation (30) between D and z now leads to a density-dependence of the unidirectional backward wave speed. The fact that this leads to an improved fit to the unidirectional data supports (30).

The continuity constraint (30) is further supported by the following cross-validation. The dashed lines in Fig. 5(c) and (d) represent the bidirectional FD when estimated from the bidirectional data only. That is, the dashed line in Fig. 5(c) is not estimated from the data points shown in that figure but only by using the data points shown in Fig. 5(d) and relying on (30). Only the maximum density is not estimated but fixed at $\hat{\varrho}/b = 6.69\,\mathrm{m}^{-2}$ because this parameter does not enter the SS regime of the bidirectional FD (29). The close coincidence of the solid and the dashed line in Fig. 5(c) over the entire density range for which data is available ($\leq 4\,\mathrm{pedestrians/m}^2$) makes a strong case in favor of the continuity constraint (30): The fit against only the unidirectional data is $R^2 = 0.85$ when estimating the model from both uni- and bidirectional data, and it is still $R^2 = 0.84$ when estimating the model only from bidirectional data. The opposite cross-validation (estimating from the uni-directional data only and then validating against the bidirectional data) led to convergence issues in the calibration. It turned out that the rather large spread in the congested branch of the unidirectional data led to an objective function that

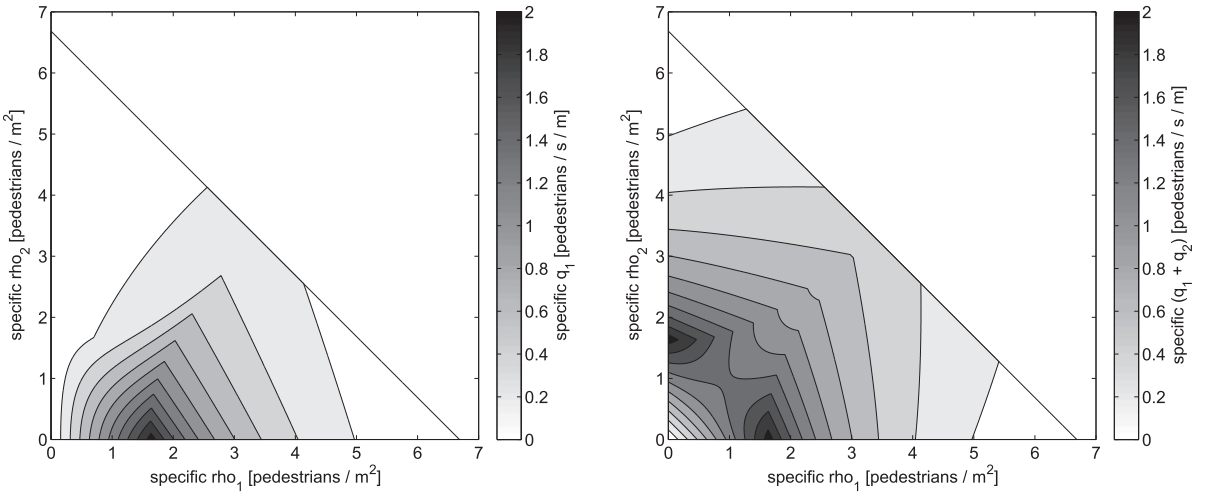

(a) Specific flow $\tilde{q}_1$ over specific densities (b) Total specific flow $\tilde{q}_1 + \tilde{q}_2$ over specific densities

Fig. 6. Aspects of FD fitted against real data. Displayed are specific flows in pedestrians per second per cross-section-meter. Darker shadings indicate higher flows.

was too flat to independently identify the three parameters β, γ, and $\hat{\varrho}$. The collection of larger datasets that allow for more comprehensive cross-validations is an important future research activity.

The assumption of a perfect 50/50 density split in the bidirectional case is a clear idealization. This adds to the previously discussed general statistical issues in that it suggests the existence of measurement errors in explanatory variables, which are another source of endogeneity and, hence, biased parameter estimates (Greene, 2003). Here, the availability of a structural FD that covers the entire bidirectional density space turns out very useful. Fig. 6(b) plots the total flow predicted by the bidirectional FD over the densities. The FD shown in Fig. 5(d) is a cut of this FD along the main diagonal. Deviations from a 50/50 density composition lead to lateral deviations from this main diagonal. While a general-purpose (say, polynomial) FD would be unable to predict the effect of such deviations due to a lack of data, the proposed structural FD is capable of making meaningful extrapolations. Qualitatively, one observes that (i) the effect of unbalanced densities is almost negligible for low densities, (ii) it leads to higher flows than predicted based on a perfect 50/50 split for intermediate densities, and (iii) it leads to lower flows than predicted for high densities. Quantitatively, one could absorb such biases by expressing the true (unobserved) density composition as a distributed quantity, which then would need to be integrated out in (46).

These experiments were, due to the unavailability of other data, constrained to the consideration of unidirectional and symmetric bidirectional flow. The proposed bidirectional FD, however, is fully capable of capturing unsymmetrical flows. This is clarified by Fig. 6(a), which shows the specific flow $\tilde{q}_1$ of direction 1 over the specific densities $(\tilde{\varrho}_1, \tilde{\varrho}_2)$. In particular, this figure supports the intuition that for a given density $\tilde{\varrho}_1$ the flow $\tilde{q}_1$ decreases monotonically as the counter-flow density $\tilde{\varrho}_2$ increases.

3.3. Consistency with other empirical phenomena

The previous analysis has already made clear that the proposed bidirectional FD satisfies the three basic requirements identified in the literature synthesis: (i) Reproducing the single-peaked shape of a unidirectional FD if one density vanishes, (ii) maintaining substantial flow levels in the balanced bidirectional case even for high densities, (iii) interpolating between unidirectional and balanced bidirectional flow based on principles rooted in pedestrian interactions.

This section explains a number of additional empirical phenomena in terms of the proposed bidirectional FD, demonstrating further the validity and versatility of this model.

3.3.1. Shuffling speed and velocity sensitivity studied by AlGadhi et al. (2002)

AlGadhi et al. (2002) analyze bidirectional pedestrian flows during the Mecca pilgrimage. They measure specific densities and velocities per direction and estimate a linear model mapping densities on velocities. A density interaction term is also tested but found insignificant; models of higher complexity are not considered. The rather low maximum velocity of $0.53\,\mathrm{m/s}$ predicted by the model may be explainable by the religious purpose of the walking. The maximum density of $5.68\,\mathrm{m}^{-2}$ predicted by the model is below the measured value of $7\,\mathrm{m}^{-2}$. Although the global validity of this simple linear model may be questioned, its parameters constitute insightful summary statistics. AlGadhi et al. (2002) make two empirical observations that can be compared to predictions of the proposed bidirectional FD.

First, AlGadhi et al. (2002) report an observed lower bound on the speed (called "shuffling speed") of 500 meters per hour, which is maintained even at very high densities. The proposed bidirectional FD captures this phenomenon. Considering only density configurations (ϱ_i, ϱ_j) with $\varrho_i + \varrho_j = \hat{\varrho}$, the model (29) yields (density-dependent) shuffling speeds between zero (vanishing counter-flow; fully congested unidirectional conditions) and $\hat{v}/(1 + D\hat{v}\hat{\varrho})$ (counter-flow density equal to or higher than own density). Solving this inequality for D and inserting the parameters $\hat{v} = 0.53\,\mathrm{m/s}$, $v^{\mathrm{shuffle}} = 0.14\,\mathrm{m/s}$, and $\hat{\varrho}/b = 7\,\mathrm{m}^{-2}$ reported by AlGadhi et al. (2002), one obtains a reasonable maximum D value of 1.24 s. That is, the proposed FD (i) reproduces the empirically observed shuffling speed and (ii) explains its magnitude through a plausible parametrization.

Second, AlGadhi et al. (2002) evaluate in their model the ratio $\left(\frac{dv_i}{d\tilde{\varrho}_i}\right)/\left(\frac{dv_i}{d\tilde{\varrho}_j}\right)$ of the derivative of the class-i velocity v_i with respect to its own density $\tilde{\varrho}_i$ and with respect to the counter-flow density $\tilde{\varrho}_j$. The resulting ratio of 2.63 leads them to the conclusion that "the impedance exerted on the average speed of a stream of pilgrims by pilgrims moving in the same direction is more than twice that of those moving in the opposite one". To obtain a corresponding prediction from the proposed FD, the parameters $\hat{v} = 0.53\,\mathrm{m/s}, \hat{\varrho}/b = 7\,\mathrm{m}^{-2}$ are again used and the functional form $D(\tilde{\varrho}_i, \tilde{\varrho}_j) = 0.39\,\mathrm{s} \cdot \left(\frac{b\tilde{\varrho}_i + b\tilde{\varrho}_j}{1\,\mathrm{m}^{-1}}\right)^{1.43}$ is, due to lacking alternative information, taken over from Section 3.2. Evaluating the derivatives $\frac{dv_i}{d\tilde{\varrho}_i}$ and $\frac{dv_i}{d\tilde{\varrho}_j}$ at the measured average densities $(\tilde{\varrho}_i, \tilde{\varrho}_j) = (2.39\,\mathrm{m}^{-2}, 0.89\,\mathrm{m}^{-2})$ yields a ratio of 3.07. Evaluating this ratio everywhere in the ellipsis with a $\tilde{\varrho}_i$-radius of $1.52\,\mathrm{m}^{-2}$ and a $\tilde{\varrho}_j$-radius of $0.68\,\mathrm{m}^{-2}$, which are twice the respective density standard deviations reported by AlGadhi et al. (2002), yields values ranging from -0.04 to 3.47. The proposed bidirectional FD hence predicts relative impedance values that are in the same order of magnitude as those observed by AlGadhi et al. (2002).

3.3.2. Capacity flows studied by Lam et al. (2002); Lam et al. (2003) and Navin and Wheeler (1969)

There exists a body of literature on bi-directional pedestrian flows that uses flows and so-called flow ratios as explanatory variables in models of, in particular, travel time. Of these, Lam et al. (2002, 2003) are particularly noteworthy because they also provide insightful summary statistics of their data. These models are, essentially, modified versions of the BPR function (Bureau of Public Roads, 1964) for road traffic, which expresses travel time as a function of flow. The bidirectional nature is inserted by making the parameters of the unidirectional BPR function dependent on the flow ratio

$$r_i = \frac{\tilde{q}_i}{\tilde{q}_i + \tilde{q}_j}, \tag{48}$$

which represents the fractional amount of direction-i flow with respect to the total channel throughput (sum of flows in both directions i and j).

Comparing this model class to the proposed bidirectional FD is similar to (but, due to the bidirectionality, more difficult than) comparing the unidirectional BPR function to a unidirectional FD of road traffic. The BPR function's well known deficiency of not correctly representing congested conditions is overcome in the FD-based approach by using densities as explanatory variables, through which uncongested and congested conditions can be separated. In order to compare a BPR function to an FD, one needs to again eliminate the explanatory density variables in the FD (or infer them in the BPR function) and constrain the analysis to uncongested conditions. These limitations in the comparison carry over to bidirectional pedestrian flows.

Lam et al. (2002) study bidirectional pedestrian flows at two different pedestrian crossings; Lam et al. (2003) study bidirectional pedestrian flows in two indoor walkways. Table 1 summarizes the real data presented in these articles. Each subfigure represents one dataset. The first column shows the flow ratio r_i. The second column shows the largest observed specific flow $\tilde{q}_i$ for a given flow ratio, which is interpreted by Lam et al. (2002, 2003) as the flow capacity of direction i under that flow ratio. The third column shows the corresponding velocity v_i.

A specific density $\tilde{\varrho}_i$ is computed in column four for each flow ratio separately from the available flow and velocity data. One observes a striking lack of density variability within each dataset. This is indeed in line with the predictions of the proposed bidirectional FD as derived in Section 2.5: Stable capacity flows are obtained at symmetric densities $\tilde{\varrho}_i = \tilde{\varrho}_j = \hat{\varrho}/2b$, with the empirical average density values being likely to be somewhat below these values. Based on this, the lower bounds on the specific jam densities in the experiments of Lam et al. (2002, 2003) would be between $3\,\mathrm{m}^{-2}$ and $6\,\mathrm{m}^{-2}$. These are reasonable numbers. Given the lack of variability in explanatory variables, a regression of the proposed bidirectional FD against any of these data sets turned out to be either infeasible or numerically extremely unstable. A further analysis of the empirical flows was also problematic: When using (48) to compute the total flow $\tilde{q}_i + \tilde{q}_j$ from $\tilde{q}_i$ and r_i in the fifth (last) column of Table 1(a)-(d), one observes that this total flow is not at all symmetric around an 0.5 flow ratio. Given that Lam et al. (2002, 2003) do not comment on possible asymmetries in their experiments, it is difficult to draw further quantitative conclusions from these data sets. A possible explanation is that the nonlinear transformation used to compute the total flow from average flows introduces a bias.

An important qualitative observation is that no flow or velocity discontinuity can be observed in these data sets when going from bidirectional ($r_i < 1$) to unidirectional ($r_i = 1$) flows. This supports the hypothesis that the continuity constraint (30) is satisfied in these data sets, which were collected on between 2.8 m and 9 m wide channels. The limited validity of the continuity constraint (30) for *narrow* channels is, on the other hand, indicated by Navin and Wheeler (1969), who study

Table 1
Lam et al. (2002, 2003) dataset summary.

r_i	$\tilde{q}_i \left[\frac{1}{\text{m}\cdot\text{min}}\right]$	$v_i \left[\frac{\text{m}}{\text{min}}\right]$	$\tilde{\varrho}_i = \frac{\tilde{q}_i}{v_i}$	$\tilde{q}_i + \tilde{q}_j = \frac{\tilde{q}_i}{r_i}$
(a) Tai Tong Road LRT Station (outdoor crossing)				
0.1	60.3	19.4	3.11	603.0
0.2	64.9	22.5	2.88	324.4
0.3	69.1	25.1	2.75	230.5
0.4	73.7	27.3	2.71	184.3
0.5	77.6	28.6	2.71	155.1
0.6	79.1	29.1	2.72	131.8
0.7	79.5	29.2	2.72	113.6
0.8	79.8	29.3	2.73	99.7
0.9	80.0	29.3	2.73	88.9
1.0	80.1	29.4	2.73	80.1
(b) Tsuen Wan Market Street (outdoor crossing)				
0.1	67.2	24.9	2.71	672.3
0.2	70.4	27.0	2.60	351.9
0.3	73.7	29.0	2.54	245.8
0.4	76.2	30.5	2.50	190.6
0.5	77.1	31.2	2.47	154.3
0.6	78.0	31.5	2.47	129.9
0.7	78.2	31.6	2.47	111.7
0.8	78.3	31.6	2.48	97.9
0.9	78.4	31.7	2.48	87.1
1.0	78.5	31.7	2.48	78.5
(c) Shatin (indoor shopping walkway)				
0.1	56.1	35.9	1.56	561.0
0.2	61.3	39.0	1.57	306.5
0.3	63.3	40.7	1.56	211.0
0.4	65.0	41.9	1.55	162.5
0.5	66.8	42.3	1.58	133.6
0.6	67.2	42.4	1.58	112.0
0.7	67.4	42.7	1.58	96.3
0.8	67.6	42.9	1.58	84.5
0.9	68.0	42.9	1.59	75.6
1.0	68.0	43.0	1.58	68.0
(d) Wan Chai (indoor commercial walkway)				
0.1	66.7	42.5	1.57	667.0
0.2	69.2	45.8	1.51	346.0
0.3	71.2	48.5	1.47	237.3
0.4	73.4	49.9	1.47	183.5
0.5	73.8	50.5	1.46	147.6
0.6	74.3	50.7	1.47	123.8
0.7	74.6	50.8	1.47	106.6
0.8	74.8	50.9	1.47	93.5
0.9	74.8	51.0	1.47	83.1
1.0	75.0	51.0	1.47	75.0

sidewalks of at most 2.4 m width. They plot channel throughput over flow composition and observe that "the points form a smooth curve until a discontinuity develops for all one-way traffic. This indicates that the effects of even a small counterflow will considerably reduce the capacity of sidewalks." It should be stressed that the observation of Navin and Wheeler (1969) is completely in line with the proposed bidirectional FD because this model *does* predict a flow discontinuity for narrow channels, where the continuity constraint (30) does not apply.

Given that the limited density variability and unexplained asymmetry in the data of Lam et al. (2002, 2003) did not allow for an estimation of the proposed FD, its quantitative explanatory power could not be investigated here. However, it could be established that the proposed FD reproduces important structural features of the data. This is an arguably even more important property for a model that has only a minimal number of parameters through which structural modeling deficiencies could be compensated.

3.3.3. *Efficiency of bidirectional flows reported by Helbing et al. (2005); Kretz et al. (2006)*

Helbing et al. (2005) present several bidirectional flow experiments in a long channel with bottlenecks of varying extension in its center. They state that "counterflows are significantly more efficient than unidirectional flows". (Similarly, Kretz et al. (2006) observe that "the sum of flow and counterflow [...] turns out to be larger than the flow in all situations without counterflow", although their pedestrian group sizes are too small to postulate stationarity.) The presence of a bottleneck within the channel and the absence of other obstacles motivates the assumption that bidirectional capacity flows arise within the bottleneck. The analysis of Section 2.5 then predicts (i) maximum density within the bottleneck and (ii) an on

average 50/50 density share within the bottleneck. Prediction (i) is supported by the photographs provided by Helbing et al. (2005). Prediction (ii) is rather natural to assume given the symmetry of the experiments.

Eq. (41) then predicts a bidirectional capacity flow of $q_i + q_j = \frac{\hat{v}\hat{\varrho}}{1+D\hat{v}\hat{\varrho}}$. The flow capacity of a symmetric triangular unidirectional FD is, on the other hand, $\frac{\hat{v}\hat{\varrho}}{2}$. Indeed, this value constitutes an upper bound for the capacity of a non-symmetric triangular FD where the maximum velocity is in absolute terms larger than the backward wave speed. The observation of Helbing et al. (2005) can hence be rephrased as $c\frac{\hat{v}\hat{\varrho}}{2} < \frac{\hat{v}\hat{\varrho}}{1+D\hat{v}\hat{\varrho}}$ with the variable $c \in (0, 1]$ expressing that the unidirectional capacity is an upper bound. Rearranging, this leads to the conclusion that any parameter configuration that satisfies the inequality $D < \frac{2/c-1}{\hat{v}\hat{\varrho}}$ with a problem-specific $c \in (0, 1]$ leads to an instance of the proposed bidirectional FD that is consistent with the empirical findings of Helbing et al. (2005) and Kretz et al. (2006).

3.3.4. Inefficiency of bidirectional flows reported by Alhajyaseen et al. (2011)

Alhajyaseen et al. (2011) study bidirectional flows at pedestrian crossings and observe that bidirectional flows are by about 25% *less* efficient than unidirectional flows. Continuing the analysis given in the previous paragraph, the observation of Alhajyaseen et al. (2011) can be explained by the proposed bidirectional FD if the conflict delay parameter satisfies the opposite inequality $D > \frac{2/c-1}{\hat{v}\hat{\varrho}}$ with a problem-specific $c \in (0, 1]$.

Alhajyaseen et al. (2011) explain their finding by the fact that the considered pedestrian crossings are too short to allow for lane formation, which would reduce the frequency of conflicts between pedestrians walking in different directions. This is in line with Helbing et al. (2005), who stresses the positive effect of lane formation on total flow throughput. The proposed bidirectional FD does not explicitly capture lane formation, which indeed could be considered more as an aspect of path choice than of flow propagation. The above discussion makes clear, however, that the model is capable of capturing the effect of lane formation (a reduction of mutual obstruction) through a suitable selection of its conflict delay parameter D. The explicit incorporation of lane formation is an important venue for future research.

Overall, further validation of the proposed model, in particular for settings with unsymmetrical density splits, is clearly desirable. However, valid datasets representing bidirectional pedestrian flows appear still difficult to access. For instance, Lee et al. (2005) tabulate (occupancy, flow, speed) triples, but these triples constitute boundary values for level-of-service classes instead of measurements and hence cannot be used for model estimation. Wong et al. (2010) map direction-specific densities on velocities but present their data in the form of three-dimensional scatter plots that render an extraction of numerical information impossible.

4. Summary and outlook

An analytical closed-form bidirectional pedestrian FD mapping direction-specific densities onto direction-specific flows was derived. The FD has the following desirable mathematical properties:

- The flows depend continuously on the model's parameters, and they depend continuously on the densities at least for strictly positive densities or for wide channels.
- The model has one and only one solution for each feasible density and parameter configuration.
- The flows are non-negative.
- Negative densities cannot be attained.
- The jam density cannot be exceeded.

The proposed FD is verified by comparison to a widely accepted pedestrian micro-simulation model and calibrated against a real data set. A very good fit is obtained in either case, despite of the model's minimal number of parameters. Further empirical phenomena reproduced by the proposed FD comprise

- the single-peaked shape of a unidirectional FD if one density vanishes;
- the persistence of substantial flow levels in the balanced bidirectional case even for high densities;
- a continuous transition between unidirectional and bidirectional flows in wide channels and a discontinuous transition between unidirectional and bidirectional flows in narrow channels;
- substantial "shuffling speeds" being maintained even at very high densities;
- the density of pedestrians moving in one direction having a larger effect on their velocity than the density of the opposite direction;
- the emergence of maximum densities, split symmetrically between the two directions, at bidirectional capacity flows;
- bidirectional flows with lane formation being more effective than unidirectional flows and bidirectional flows without lane formation being less effective than unidirectional flows.

A structural relationship between two collision avoidance parameters (the safety gap to a lead pedestrian and the conflict delay resulting from moving around a counter-flow pedestrian) is established based on (i) behavioral considerations and (ii) comparisons to real data, including a cross-validation. The practical importance of this relationship stems from the fact that

it provides a one-on-one mapping between uni- and bidirectional pedestrian FD parameters. It must, however, be stressed that this continuity constraint is a modeling assumption, and as such it may be dropped if empirical or other evidence against it does not support this assumption. This is likely to be the case for very narrow channels. Removing the continuity constraint leaves the proposed FD completely intact.

The derivation of models for more general topologies – networks of channels or even two-dimensional systems – appears feasible based on the same approach as taken here, starting from an intuitive CA specification and then deriving a continuum approximation.

The unidirectional CA/KWM equivalence result of Daganzo (2006) motivates the development of dynamical model versions: The proposed bidirectional FD can be reformulated as a system of unidirectional FDs, with each unidirectional FD taking the density and flow of the other direction as additional parameters, cf. (35)–(38). This suggests the feasibility of inserting the proposed FD into a bidirectional KWM. This bidirectional KWM could symmetrically be expressed as a system of unidirectional KWMs, with each unidirectional sending and receiving function taking the density and flow of the other direction as additional (time- and space-dependent) parameters. Numerical solution schemes for the unidirectional formulation are readily available, foremost the cell-transmission model (Daganzo, 1994).

Acknowledgment

This work was partially supported by the PETRA project, funded by the European Commission 7th Framework Programme (FP7-SMARTCITIES-2013) under project number 609042.

References

AlGadhi, S., Mahmassani, H., Herman, R., 2002. A speed-concentration relation for bi-directional crowd movements with strong interaction. In: Schreckenberg, M., Sharma, S. (Eds.), Pedestrian and Evacuation Dynamics. Springer, Berlin, Germany, pp. 3–20.

Alhajyaseen, W., Nakamura, H., Asano, M., 2011. Effects of bi-directional pedestrian flow characteristics upon the capacity of signalized crosswalks. In: Procedia – Social and Behavioral Sciences 16, 526–535, 6th International Symposium on Highway Capacity and Quality of Service.

Ansorge, R., 1990. What does the entropy condition mean in traffic flow theory. Transportation Research Part B 24 (2), 133–143.

Appert-Rolland, C., Degond, P., Motsch, S., 2014. A macroscopic model for bidirectional pedestrian flow. In: Weidmann, U., Kirsch, U., Schreckenberg, M. (Eds.), Pedestrian and Evacuation Dynamics 2012. Springer, Cham, pp. 575–583.

Asano, M., Sumalee, A., Kuwahara, M., Tanaka, S., 2007. Dynamic cell transmission-based pedestrian model with multidirectional flows and strategic route choices. Transportation Research Record 2039, 42–49.

Baek, S., Minnhagen, P., Bernhardsson, S., Choi, K., Kim, B., 2009. Flow improvement caused by agents who ignore traffic rules. Physical Review E 80 (1), 016111.

Blue, V., Adler, J., 1998. Emergent fundamental pedestrian flows from cellular automata microsimulation. Transportation Research Record 1644, 29–36.

Blue, V., Adler, J., 2000a. Cellular automata model of emergent collective bi-directional pedestrian dynamics. In: Berdau, M., McCaskill, J., Packard, N., Rasmussen, S. (Eds.), Proceedings Artificial Life VII. MIT press, Cambridge MA, USA, pp. 437–445.

Blue, V., Adler, J., 2000b. Modeling four-directional pedestrian flows. Transportation Research Record 1710, 20–27.

Blue, V., Adler, J., 2001. Cellular automata microsimulation for modeling bi-directional pedestrian walkways. Transportation Research Part B 35 (3), 293–312.

Bureau of Public Roads, 1964. Traffic Assignment Manual. US Department of Commerce, Urban Planning Divisions, Washington, DC.

Cheung, C., Lam, W., 1997. A study of the bi-directional pedestrian flow characteristic in Hong Kong mass transit railway stations. Journal of the East Asian Society for Transportation Studies 2 (5), 1607–1619.

Chraibi, M., Seyfried, A., Schadschneider, A., 2010. Generalized centrifugal-force model for pedestrian dynamics. Physical Review E 82 (4), 046111.

Daganzo, C., 1994. The cell transmission model: a dynamic representation of highway traffic consistent with the hydrodynamic theory. Transportation Research Part B 28 (4), 269–287.

Daganzo, C., 1995. The cell transmission model, part II: network traffic. Transportation Research Part B 29 (2), 79–93.

Daganzo, C., 2006. In traffic flow, cellular automata = kinematic waves. Transportation Research Part B 40 (5), 396–403.

Fruin, J., 1971. Pedestrian Planning and Design. Metropolitan Association of Urban Designers and Environmental Planners Inc., New York.

Fukui, M., Ishibashi, Y., 1999. Jamming transition in cellular automaton models for pedestrians on passageway. Journal of the Physical Society of Japan 68 (11), 3738–3739.

Goffman, E., 1971. Relations in Public: Microstudies of the Public Order. Basic Books, New York, USA.

Greene, W.H., 2003. Econometric Analysis, 5th ed. Prentice Hall, Upper Saddle River, NJ.

Guo, R.-Y., Huang, H.-J., Wong, S., 2011. Collection, spillback, and dissipation in pedestrian evacuation: a network-based method. Transportation Research Part B 45 (3), 490–506.

Hänseler, F.S., Bierlaire, M., Farooq, B., Mühlematter, T., 2014. A macroscopic loading model for time-varying pedestrian flows in public walking areas. Transportation Research Part B 69 (0), 60–80.

Helbing, D., Buzna, L., Johansson, A., Werner, T., 2005. Self-organized pedestrian crowd dynamics: experiments, simulations and design solutions. Transportation Science 39 (1), 1–24.

Helbing, D., Farkas, I., Vicsek, T., 2000. Simulating dynamical features of escape panic. Nature 407 (28), 487–490.

Helbing, D., Molnár, P., 1995. Social force model for pedestrian dynamics. Physical review E 51 (5), 4282–4286.

Isobe, M., Adachi, T., Nagatani, T., 2004. Experiment and simulation of pedestrian counter flow. Physica A: Statistical Mechanics and its Applications 336, 638–650.

Johansson, A., Helbing, D., Shukla, P., 2007. Specification of the social force pedestrian model by evolutionary adjustment to video tracking data. Advances in Complex Systems 10 (suppl. 2), 271–288.

Kirchner, A., Klüpfel, H., Nishinari, K., Schadschneider, A., 2003a. Simulation of competitive egress behavior: comparison with aircraft evacuation data. Physica A: Statistical Mechanics and its Applications 324 (3), 689–697.

Kirchner, A., Nishinari, K., Schadschneider, A.S.M., 2003b. Friction effects and clogging in a cellular automaton model for pedestrian dynamics. Physical Review E 67 (5), 056122.

Köster, G., Treml, F.M.G., 2013. Avoiding numerical pitfalls in social force models. Physical Review E 87 (6), 063305.

Kretz, T., Grünebohm, A., Kaufman, M., Mazur, F., Schreckenberg, M., 2006. Experimental study of pedestrian counterflow in a corridor. Journal of Statistical Mechanics 2006 (10), P10001.

Lam, W., Lee, J., Cheung, C., 2002. A study of the bi-directional pedestrian flow characteristics and Hong Kong signalized crosswalk facilities. Transportation 29 (2), 169–192.

Lam, W., Lee, J., Goh, C., 2003. A generalised function for modeling bi-directional flow effects on indoor walkways in Hong Kong. Transportation Research Part A 37 (9), 789–910.
Laval, J., Leclercq, L., 2013. The Hamilton–Jacobi partial differential equation and the three representations of traffic flow. Transportation Research Part B 52 (0), 17–30.
Lebacque, J., July 1996. The Godunov scheme and what it means for first order traffic flow models. In: Lesort, J.-B. (Ed.), Proceedings of the 13th International Symposium on Transportation and Traffic Theory. Pergamon, Lyon, France, pp. 647–677.
Lee, J.P.K.G., Lam, W., 2005. New level-of-service standard for signalized crosswalks with bi-directional pedestrian flows. Journal of Transportation Engineering – ASCE 131 (12), 957–960.
Lighthill, M., Witham, J., 1955. On kinematic waves II. A theory of traffic flow on long crowded roads. Proceedings of the Royal Society A 229 (1178), 317–345.
Løvås, G., 1994. Modeling and simulation of pedestrian traffic flow. Transportation Research Part B 28 (6), 429–443.
Moussa, N., 2008. Simon-Gutowitz bidirectional traffic model revisited. Physics Letters A 372 (45), 6701–6704.
Muramatsu, M., Irie, T., Nagatani, T., 1999. Jamming transition in pedestrian counter flow. Physica A 267 (3–4), 487–498.
Muramatsu, M., Nagatani, T., 2000. Jamming transition in two-dimensional pedestrian traffic. Physica A 275 (1–2), 201–281.
Nagai, R., Fukamachi, M., Nagatani, T., 2005. Experiment and simulation for counterflow of people going on all fours. Physica A 358 (2–4), 516–528.
Nagel, K., Schreckenberg, M., 1992. A cellular automaton model for freeway traffic. Journal de Physique I France 2 (12), 2221–2229.
Navin, P., Wheeler, R., 1969. Pedestrian flow characteristics. Traffic Engineering 19 (7), 30–33,3.
Nowak, S., Schadschneider, A., 2012. Quantitative analysis of pedestrian counterflow in a cellular automaton model. Physical Review E 85 (6), 066128.
Older, S., 1968. Movement of pedestrians on footways in shopping streets. Traffic Engineering and Control 10 (4), 160–163.
Pushkarev, B., Zupan, J., 1975. Urban Space for Pedestrians: A Report of the Regional Plan Association. MIT Press, Cambridge MA, USA.
Richards, P., 1956. Shock waves on highways. Operations Research 4 (1), 42–51.
Rickert, M., Nagel, K., Schreckenberg, M., Latour, A., 1996. Two lane traffic simulations using cellular automata. Physica A 231 (4), 534–550.
Schadschneider, A., 1998. Analytical approaches to CA for traffic flow: approximations and exact solutions. In: Schreckenberg, M., Wolf, D. (Eds.), Traffic and Granular Flow '97. Springer.
Shukla, P., 2010. On medeling and evolutionary optimization of nonlinearly coupled pedestrian interactions. In: Groos, G., Hartmanis, J., van Leeuwen, J. (Eds.), Applications of Evolutionary Computation. No. 6024 in Lecture Notes in Computer Science. Springer, pp. 21–30.
Simon, P., Gutowitz, H., 1998. Cellular automaton model for bidirectional traffic. Physical Review E 57 (2), 2441–2444.
Steffen, B., Seyfried, A., 2010. Methods for measuring pedestrian density, flow, speed and direction with minimal scatter. Physica A 389 (9), 1902–1910.
Tajima, Y., Takimoto, K., Nagatani, T., 2002. Pattern formation and jamming transition in pedestrian counter flow. Physica A 313 (3–4), 709–723.
Weidmann, U., 03 1993. Transporttechnik der Fussgänger. Tech. rep., Institut für Verkehrsplanung und Transportsysteme, ETH Zürich, ETH-Hönggerberg, CH-8093 Zürich, in German.
Wong, S., Leung, W., Chan, S., Lam, W., Yung, N., Liu, C., Zhang, P., 2010. Bidirectional pedestrian stream model with oblique intersecting angle. Journal of Transportation Engineering – ASCE 136 (3), 234–242.
Xie, S., Wong, S., 2014. A Bayesian inference approach to the development of a multidirectional pedestrian stream model. Transportmetrica A: Transport Science, forthcoming.
Xie, S., Wong, S., Lam, W., Chen, A., 2013. Development of a bidirectional pedestrian stream model with an oblique intersecting angle. Journal of Transportation Engineering – ASCE 139 (7), 678–685.
Zanlungo, F., Ikeda, T., Kanda, T., 2011. Social force model with explicit collision prediction. EPL (Europhysics Letters) 93 (6), 68005.
Zhang, J., 2012. Pedestrian Fundamental Diagrams: Comparative Analysis of Experiments in Different Geometries. Phd Thesis. Universität Wuppertal, Jülich.
Zhang, J., Klingsch, W., Schadschneider, A., Seyfried, A., 2011. Transitions in pedestrian fundamental diagrams of straight corridors and t-junctions. Journal of Statistical Mechanics 2011 (06), P06004.
Zhang, J., Klingsch, W., Schadschneider, A., Seyfried, A., 2012. Ordering in bidirectional pedestrian flows and its influence on the fundamental diagram. Journal of Statistical Mechanics 2012 (02), P02002.
Zhang, J., Seyfried, A., 2014. Comparison of intersecting pedestrian flows based on experiments. Physica A 405, 316–325.
Zheng, X., Zhong, T., Liu, M., 2009. Modeling crowd evacuation of a building based on seven methodological approaches. Building and Environment 44 (3), 437–445.